Supporting Information

Constructing host-guest recognizable electrolytes promotes the Li^+ kinetics in solid-state batteries

Qing Liu,[a] Li Yang,[a] Zhiyuan Mei,[a] Qi An,[a] Kun Zeng,[a] Wenjing Huang,[a] Shimin Wang,[a] Yongjiang Sun,[a] Hong Guo,[a, b, *]

[a] School of Materials and Energy, International Joint Research Center for Advanced Energy Materials of Yunnan Province, Yunnan Key Laboratory of Carbon Neutrality and Green Low-carbon Technologies, Yunnan University, Kunming 650091, China

[b] Southwest United Graduate School, Kunming 650091, China

*Corresponding author:

guohong@ynu.edu.cn (Hong Guo)

Experimental Section

Synthesis of the cathode and anode electrodes

The cathode was prepared by blending the commercial $LiFePO_4$(LFP)/ $LiNi_{0.9}Co_{0.05}Mn_{0.05}O_2$ (NCM90) powders, carbon black (Super P) and polyvinylidene fluoride (PVDF) with a mass ratio of 90: 5: 5. The anode consisted of 90 wt % commercial graphite (S450, Shenzhen BTR New Energy Material Co., Ltd. (China)), 5 wt % conductive carbon (Super P), and 5 wt % PVDF. Then it is mixed with an appropriate amount of N-methyl pyrrolidone (NMP) solvent to form a uniform slurry.

The cathode and anode slurries were pasted onto the Al collector and copper collector, respectively. The foil was roll-pressed at a pressure of 3.5 kN after solvent drying. Subsequently, the electrodes are punched into the disks, and after an additional 8 hours of vacuum drying at 120°C, which can be used to assemble half and full cells. The diameters of a circular shape electrodes are 14 mm. The prepared LFP or NCM90 cathodes with mass loadings of 3.8~4.2 mg cm^{-2}.

Battery assembly

All the batteries were assembled in a glovebox using 2025-type coin batteries and Celgard 2400 separator. The amount of electrolyte in each cell was about 40 uL. The stainless steel symmetric batteries are assembled to test the intrinsic impedance value of the electrolyte to calculate its lithium-ion conductivity. The stainless steel working electrode with Li counter and reference electrode were used for linear sweep voltammetry (LSV) measurement. The Li|Li symmetrical coin battery is assembled with two lithium foils with a radius of 7.5 mm to test the stability of lithium-ion transport in the electrolyte and the degree of interfacial polarization. Coin-type half-cells with as-prepared electrolytes were assembled with LFP and NCM90 as working electrode, lithium foil (Tianjin China Energy Lithium Co., Ltd. (China)) as counter electrode. In addition, the coin-type full-cells of NCM90|graphite also applied to evaluate the electrochemical properties of electrolytes. The as prepared electrolytes were fabricated with N/P values of ~1.2 (calculated according to 360 mAh g^{-1} and 200 mA h g^{-1} for graphite and NCM90, respectively).

Material Analysis

The structure of all samples was identified by X-ray diffraction (XRD) (Bruker D8, Japan) in the scanning range between 10 °C and 70 °C at a rate of 5° min^{-1}. Specific surface area and pore analyzer were evaluated by BJH and BET method (3H-2000PS1/2, Beishide Instrument-S&T Co. Ltd., China). The thermogravimetric analysis (TGA) (Mettler-Toledo) was conducted in nitrogen from 50 °C to 400 °C at a heating rate of 10 °C min^{-1}. Morphological images of all samples were observed by scanning electron microscopy (SEM) (Zeiss Gemini 500, Germany) and high-resolution transmission electron microscopy (HRTEM) (JEM-2100, Japan). X-ray photoelectron spectroscopy (XPS) (Al-Kα, Thermo Fisher Scientific Co. Ltd., USA) was used to analysis the chemical compositions of samples. Young's modulus morphologies images were acquired from commercial Atomic force microscopy (AFM) (Bruker Dimension Icon). In-situ Raman (RM-1000, Renishaw) and In-situ Fourier transform infrared FTIR spectra (Nicolet IS10, USA) testing were employed to investigate the dynamic changes of polymer functional groups during electrolyte charging and discharging. The growth of Li dendrites was in situ characterized by the optical microscope (Zoom 650, Shanghai Tuming Optical Instrument Co., Ltd). The gassing behavior of cell was studied via the in-situ differential electrochemical mass spectrometry (DEMS) system (HPR-20, Hiden Analytical Ltd.), and argon was selected as inert carrier gas.

Electrochemical Measurements

Galvanostatic tests were conducted on NEWARE battery test system (CT-4008-5V50mA-164 laboratory instrument). Electrochemical impedance spectroscopy (EIS) and the LSV were conducted using an electrochemical workstation (CHI760E). Specifically speaking, LSV measurement was obtained from 2.5 to 6 V at a scan rate of 0.1 mV s^{-1}. EIS measurements were conducted to investigate the interfacial evolution. The conductivity of Li^+ ion σ was calculated by the following formula:

$$\sigma = d / SR$$

where σ is ionic conductivity, L is the pellet thickness, S is the pellet area, and R is the resistance obtained from the measurement.

The lithium-ion transference number (t_{Li^+}) was calculated by the following formula:

$$t_{Li+} = \frac{I_s(\Delta V - I_0 R_0)}{I_0(\Delta V - I_s R_s)}$$

Where ΔV is the polarization potential used in the test (10 mV), I_0 and I_s are the initial and steady-state currents, and R_0 and R_s are the first and last resistances, respectively.

Computational Details

All calculations were performed by density functional theory (DFT) using the CASTEP code[S1]. The projector augmented wave (PAW) method and plane wave basis sets were used. The Perdew-Burke-Ernzerh (PBE) functional was used within the Generalized Gradient Approximation (GGA)[S2]. After the convergence test, and the energy cutoff for the plane wave basis set was 520 eV. Structural optimizations were performed by minimizing the forces on all the atoms to below 0.01 eV·$Å^{-1}$ and the energy to below 10^{-6} eV. The electron states were sampled using a 3×3×2 k-point mesh of Γ-centered[S3].

The slab models were adopted to implement the electronic structure and thermodynamic calculation. Vacuum layer in slab model was set to 15 Å. The climbing image nudged elastic band (CI-NEB)[S4] algorithm was introduced to evaluate the migration energy barriers of diffusing atoms, inserting five images between the initial and final configurations and optimizing in all directions until convergence. Furthermore, the LOBSTER codes are introduced to calculate the Crystal Orbital Hamilton Population (COHP) of Li-O bonds[S5-S7].

References

[S1] M. D. Segall, Philip J. D. Lindan, M. J. Probert, C. J. Pickard, P. J. Hasnip, S. J. Clark and M. C. Payne, *J. Phys.: Condens. Matter*, 2002, **14**, 2717-2744.

[S2] J. P. Perdew, K. Burke and Y. Wang, Phys. Rev. B, 1996, **54**, 16533-16539.

[S3] J. D. Pack and H. J. Monkhorst, *Phys. Rev. B*, 1977, **16**, 1748-1749.

[S4] G. Henkelman, B. P. Uberuaga and H. Jonsson, J. Chem. Phys., 2000, **113**, 9901.

[S5] R. Dronskowski and P. E. Blöchl, *J. Phys. Chem.*, 1993, **97**, 8617-8624.

[S6] V. L. Deringer, A. L. Tchougréeff and R. Dronskow-ski, *J. Phys. Chem. A*, 2011, **115**, 5461-5466.

[S7] S. Maintz, V. L. Deringer, A. L. Tchougréeff and R. Dronskowski, *J. Comput. Chem.*, 2013, **34**, 2557-2567.

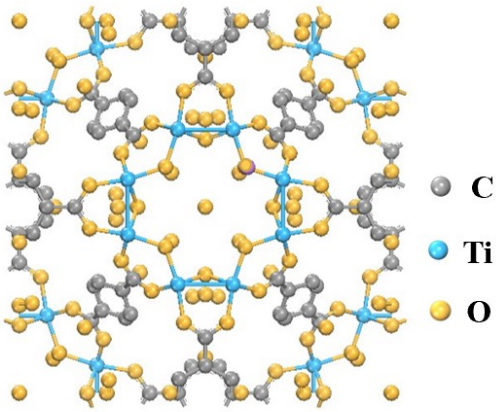

Fig. S1 Crystal structures of MOFs(Ti).

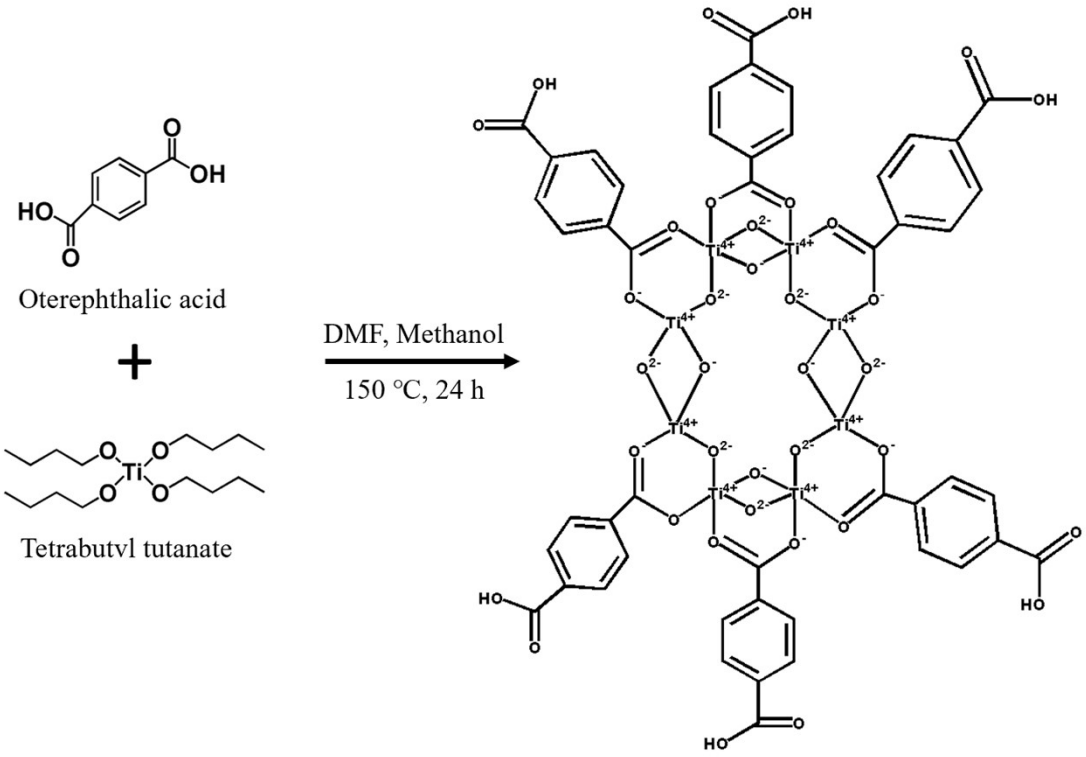

Fig. S2 The schematic diagram of reaction mechanism.

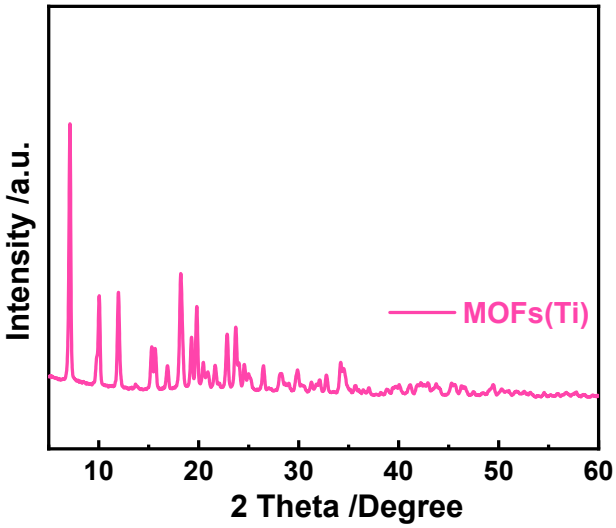

Fig. S3 XRD spectrum of MOFs(Ti) powders.

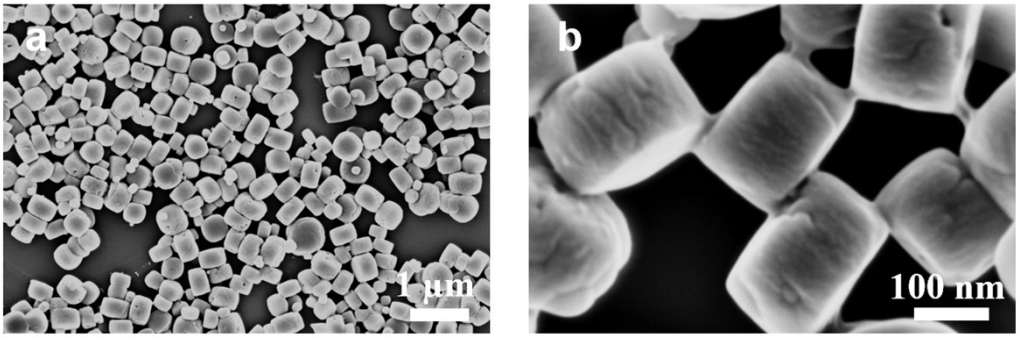

Fig. S4 SEM morphology of MOFs(Ti) powders.

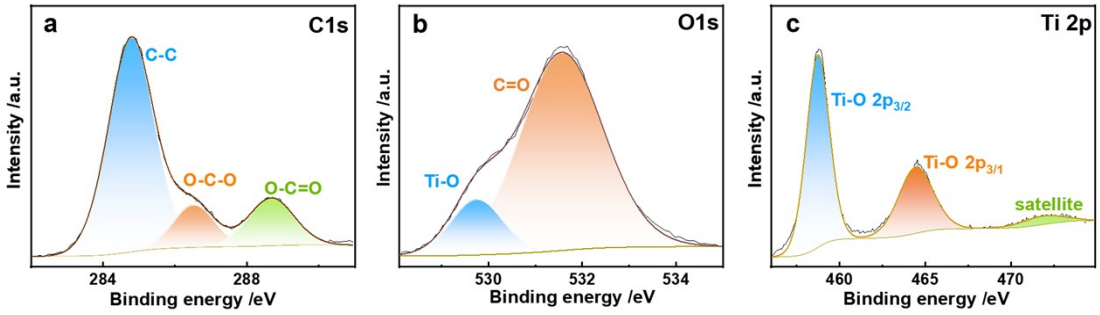

Fig. S5 XPS spectrum of (a) C1s, (b) O1s and (c) Ti2p element distribution data in MOFs(Ti) powders.

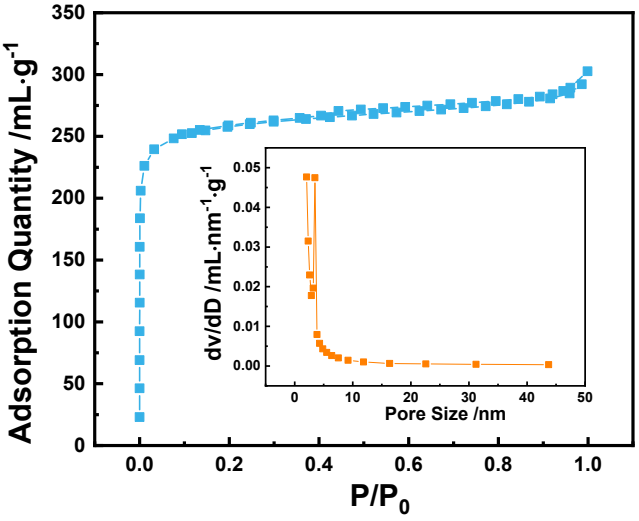

Fig. S6 The BET curves of MOFs(Ti) powders.

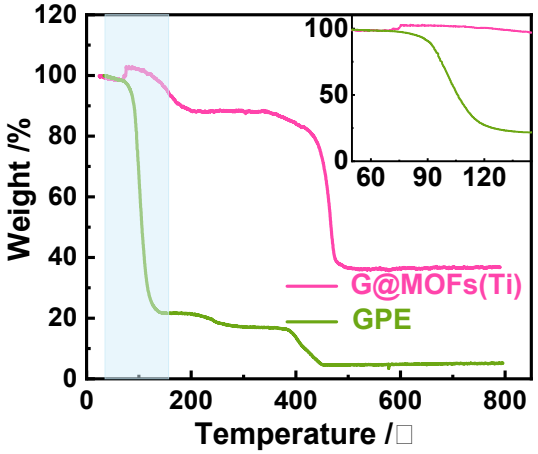

Fig. S7 The TGA curves of GPE and G@MOFs(Ti) electrolyte.

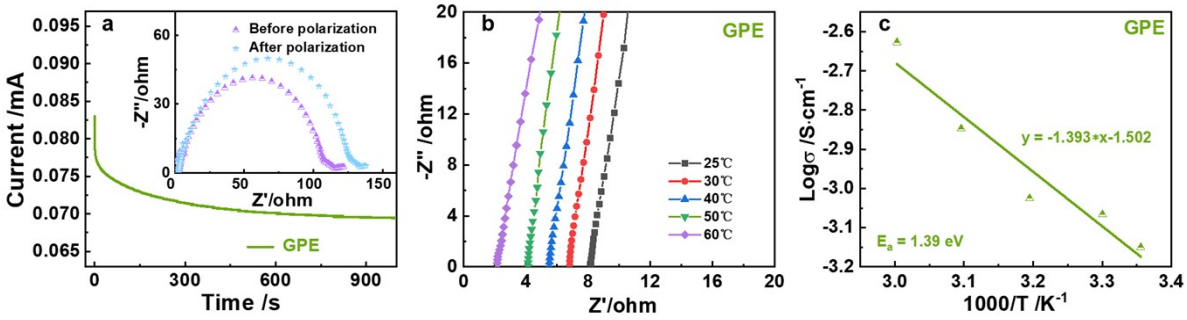

Fig. S8 (a) Chronoamperometric curves of GPE (inset displays the EIS curves before and after polarization), (b) Ionic conductivities of GPE at 25-60 °C, (c) the corresponding Arrhenius plot in inset.

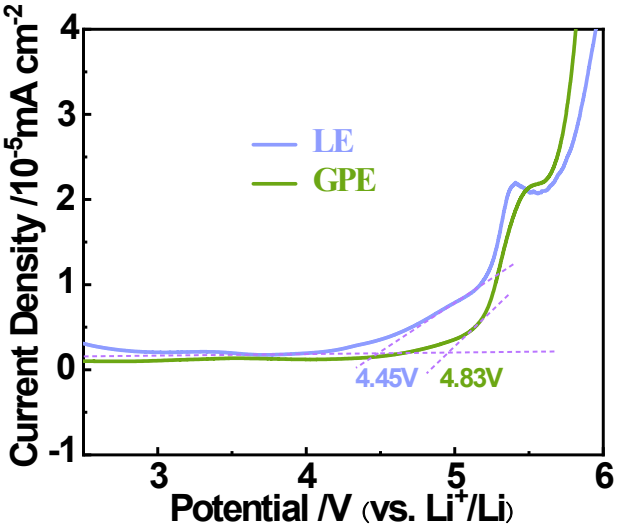

Fig. S9 The LSV curves of LE and GPE.

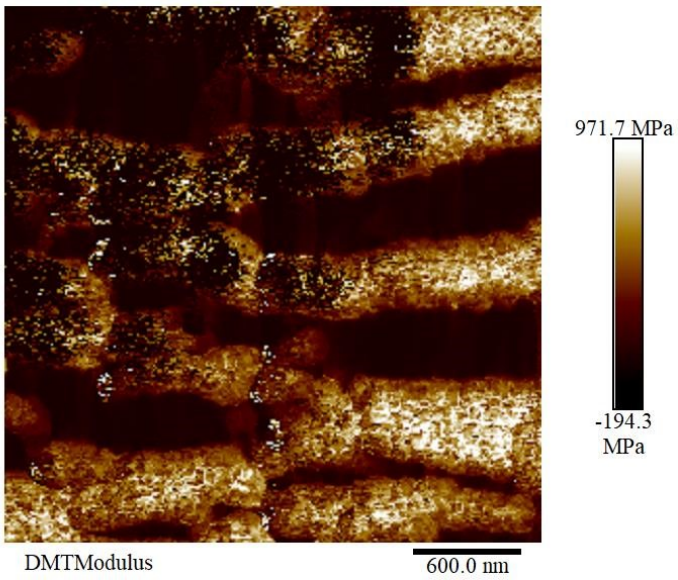

Fig. S10 Young's modulus image of GPE.

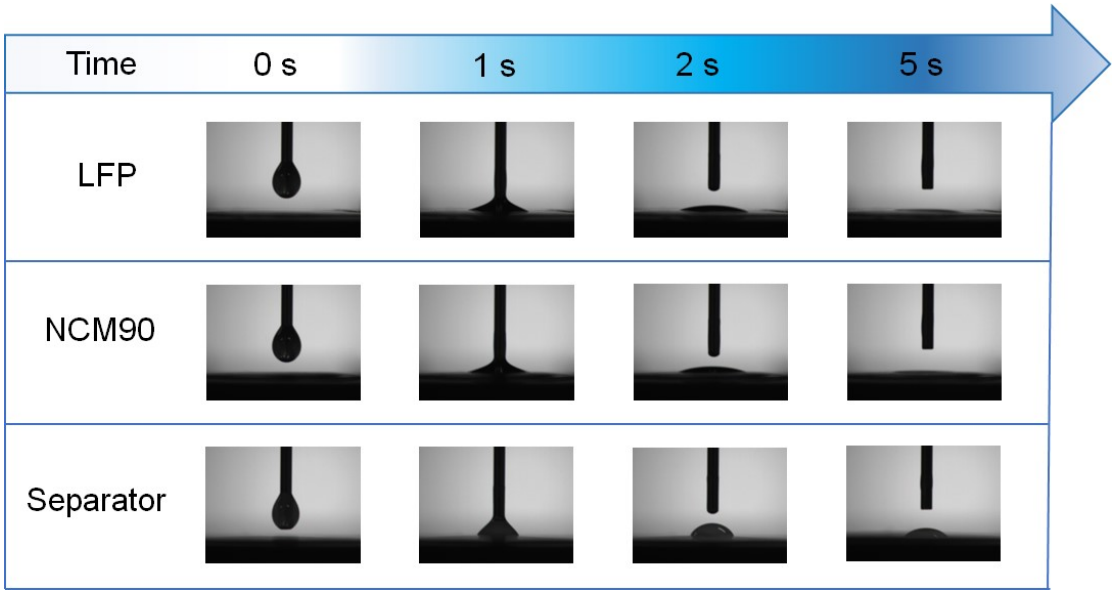

Fig. S11 Contact angle measurement of the G@MOFs(Ti) electrolyte precursor on different substrates.

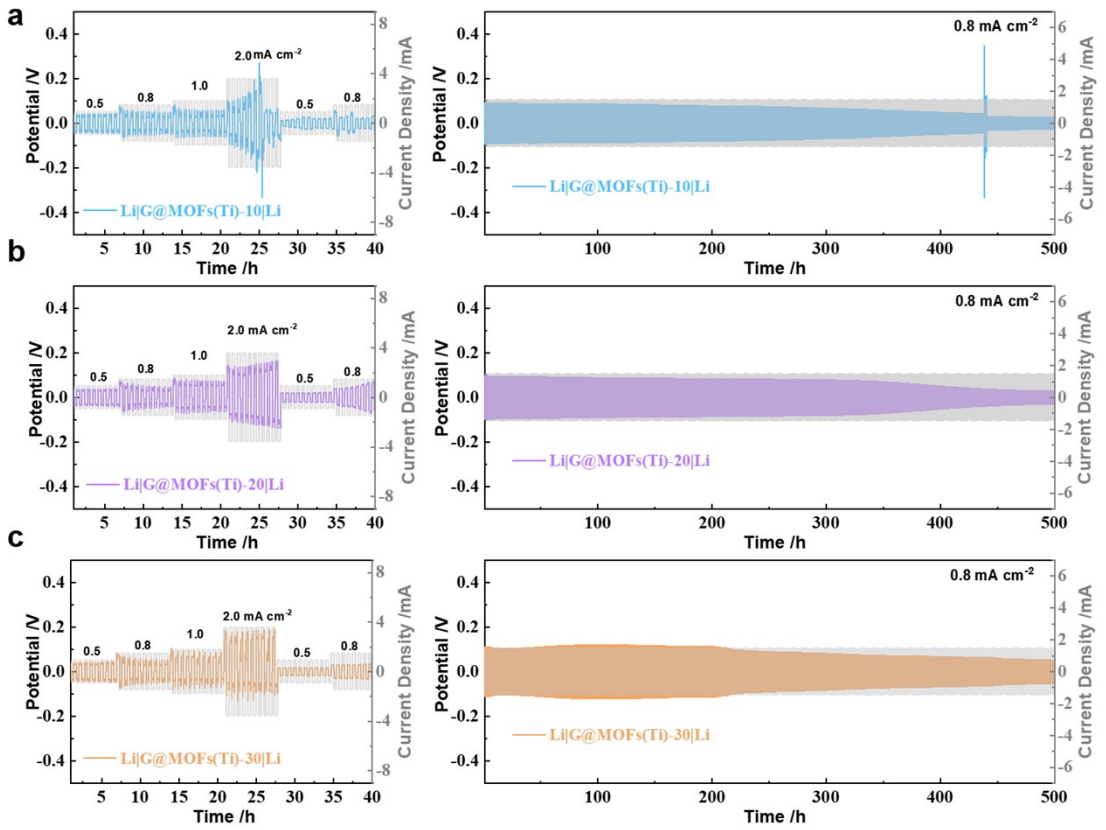

Fig. S12 The Li|Li symmetric cell performance of (a) G@MOFs(Ti)-10, (b) G@MOFs(Ti)-20, (c) G@MOFs(Ti)-30.

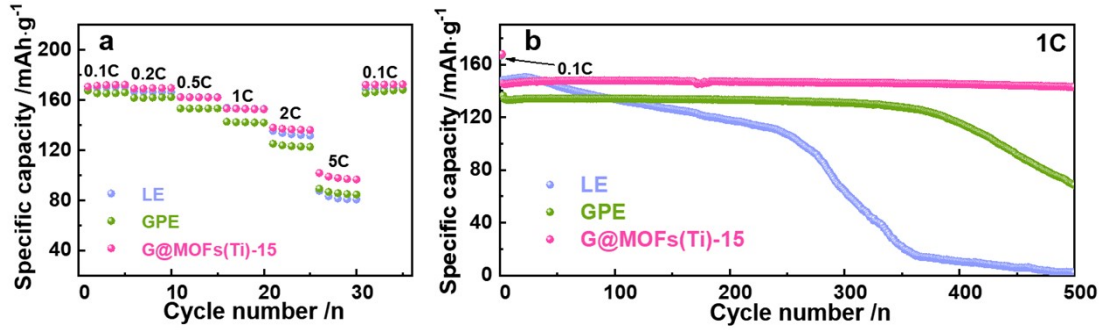

Fig. S13 The real-time optical images of the in-situ Li deposition on the Li electrode by used (a) LE electrolyte and (b) GPE electrolyte.

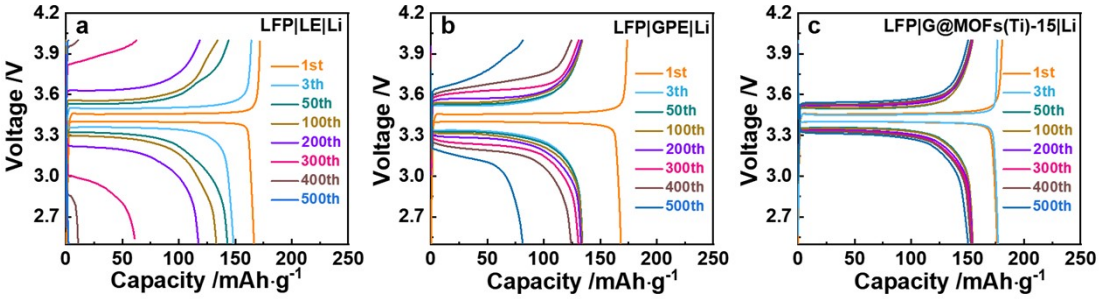

Fig. S14 The voltage platform of (a) LFP|LE|Li, (b) LFP|GPE|Li and (c) LFP|G@MOFs(Ti)-15|Li at different cycles.

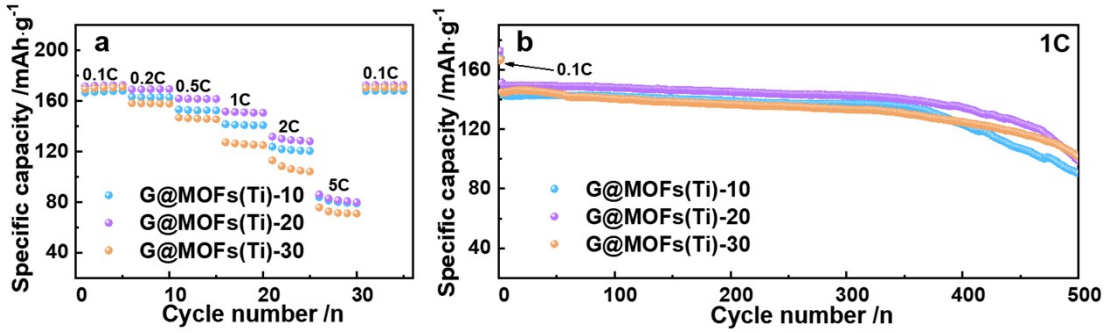

Fig. S15 The (a) rate performance and (b) long cycle performance of LFP|Li batteries assembled based on electrolytes with different contents of MOFs(Ti).

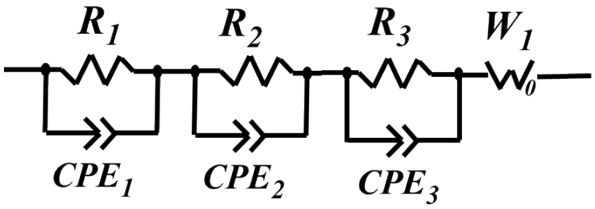

Fig. S16 The equivalent circuits of the LFP|Li cells.

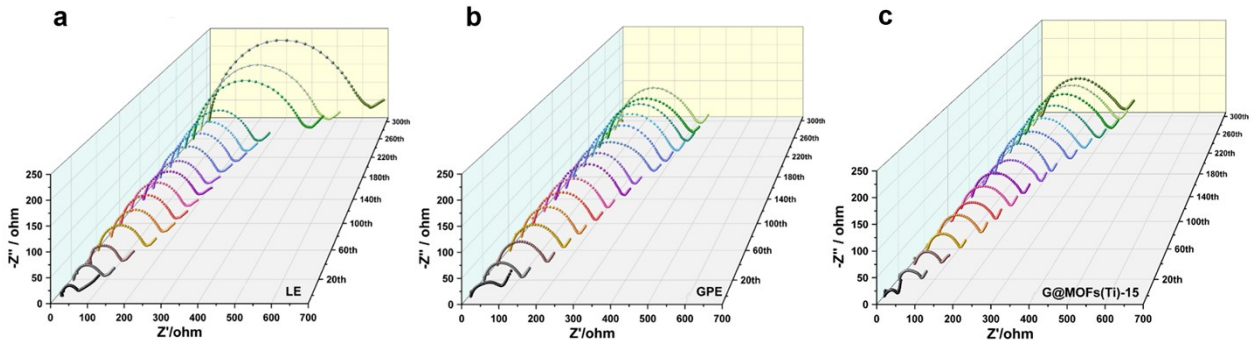

Fig. S17 The quasi-in-situ EIS of (a) LFP|LE|Li, (b) LFP|GPE|Li and (c) LFP|G@MOFs(Ti)-15|Li cells.

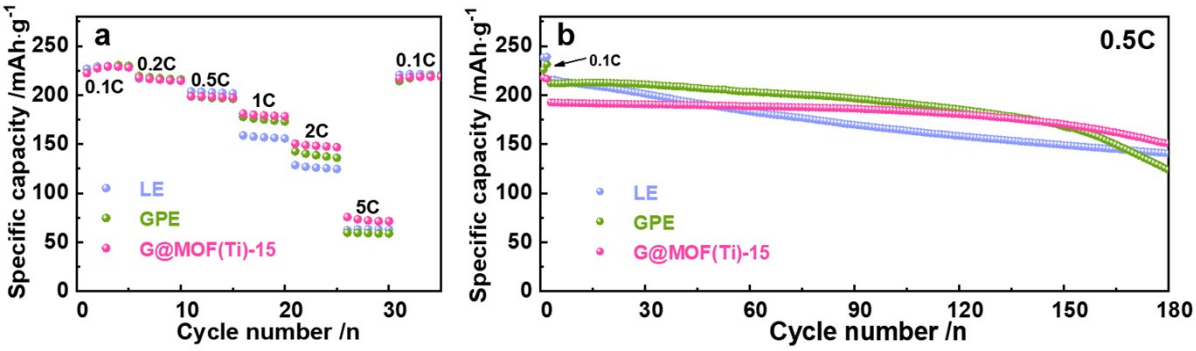

Fig. S18 (a) Rate performance and (b) long cycle performance of the NCM90|Li batteries assembled with LE, GPE and G@MOFs(Ti)-15 as electrolytes, respectively.

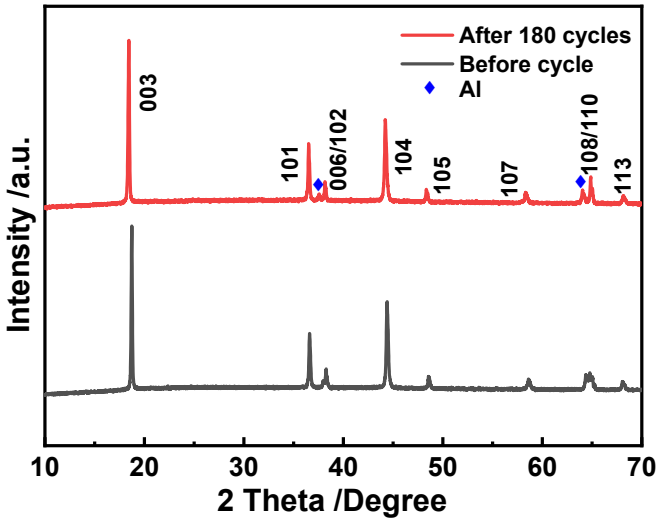

Fig. S19 The XRD spectrum of NCM90 cathode used in G@MOFs(Ti)-15 electrolyte system (a) before and (b) after cycling.

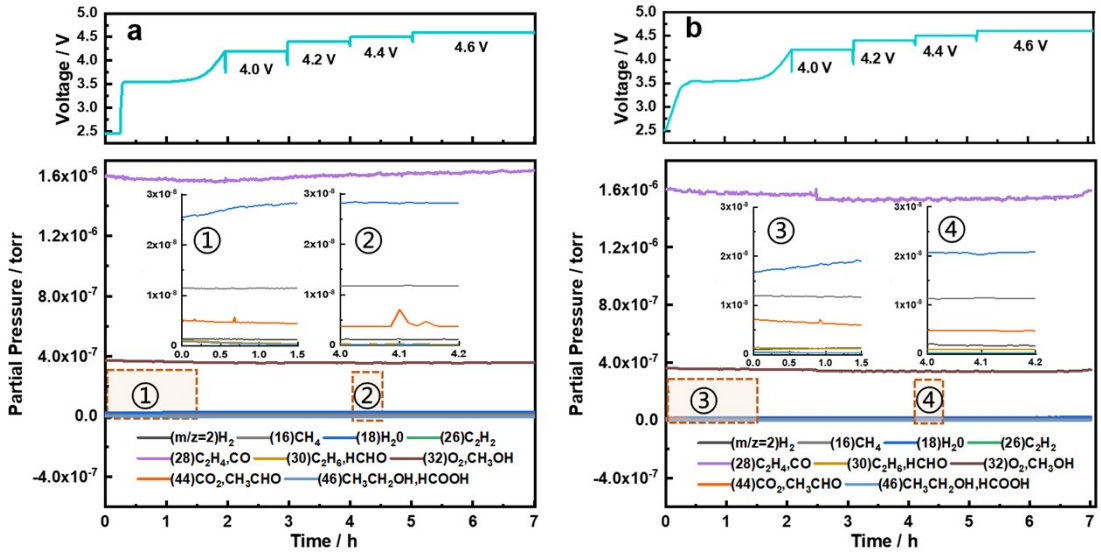

Fig. S20 Various gas generation profiles of (a) NCM90|LE|Li and (b) NCM90|GPE|Li batteries were tested by in situ DEMS.

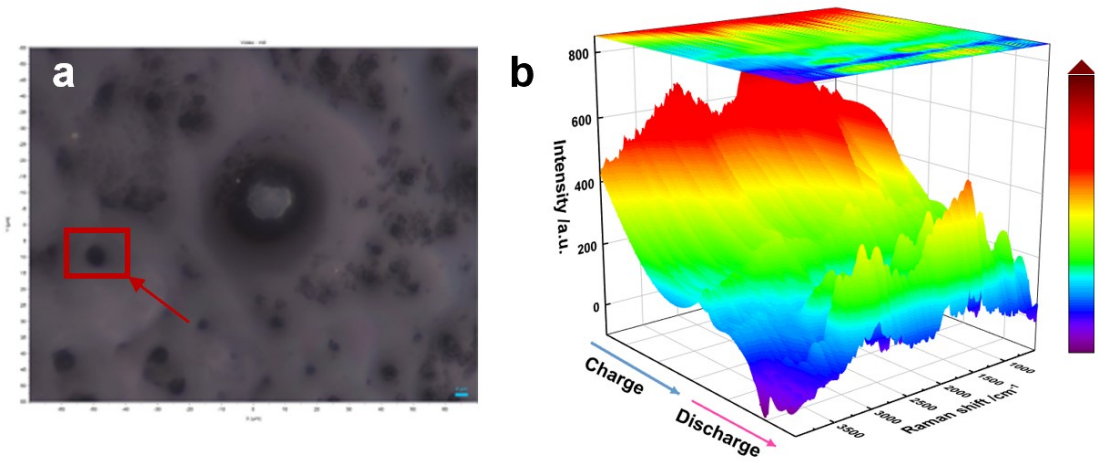

Fig. S21 (a) Selection position of in-situ Raman spectrum test, and (b) 3D diagram of Raman test results during the charge and discharge process.

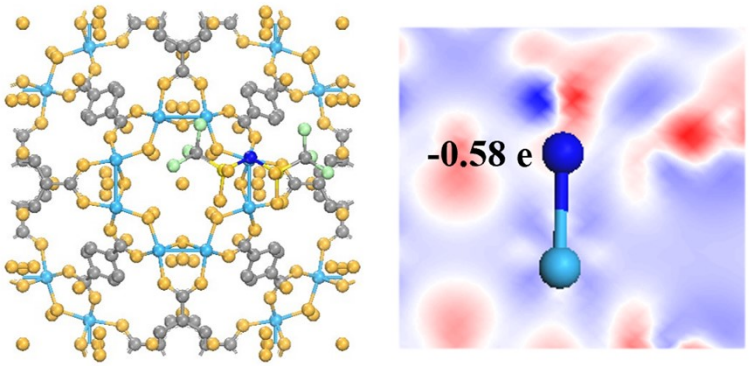

Fig. S22 Schematic diagram of electron transfer from the central N atom of the TFSI anion to the Ti site.

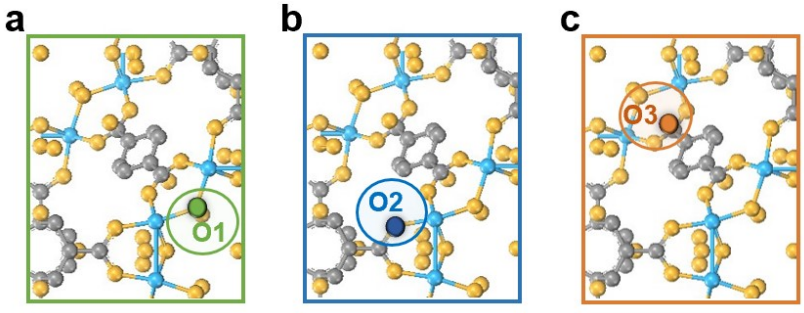

Fig. S23 The chemical positions of the three types of O.

Table S1 Performances comparison with the previously reported electrolyte systems.

Electrolytes	Cathodes	Rate Performance (mAh g^{-1})						Cycle Performance	References
		0.1C	0.2C	0.5C	1C	2C	5C		
Zn-MOF-74	LFP	152		117	94			0.5 C, 500 cycles, 90%	[25]
M-S-PEGDA	LFP	152.5	138.2	120.2	93			0.5C, 500 cycles, 85.6%	[40]
Li-Cuboct-H	LFP	143	132	125	117	97		1C, 500 cycles, 93%	[41]
DEG-PMCOF	LFP	157.8		34.7				0.2C, 100 cycles, 99.3%	[42]
	NCM622		165.9		85.1				
LGZ	LFP	124.3	115.1	103.5	90.4	64.7		1C, 500 cycles, ~100%	[43]
SE-4Cl-Li	LFP	158	153	134	111			0.5C, 50 cycles, 93.1%	[31]
	NCM811		202	191	177			0.5C, 100 cycles, 83%	
PEO/MOFs-NH	LFP				132.3			0.3C, 200 cycles, 99.2%	[44]
	NCM523		138.1					0.2C, 100 cycles, 71%	
MOFs-GPE	LFP	168.5	166.7	166.2	153.1	138	101.7	1C, 500 cycles, 98.1%	This work
	NCM90	216.9	214.6	197.8	181.3	154.3	75.7	0.5C, 100 cycles, 93.7% 250 cycles, 71.4%	